Journal of Organometallic Chemistry 880 (2019) 355–362

Contents lists available at ScienceDirect

Journal of Organometallic Chemistry

journal homepage: www.elsevier.com/locate/jorganchem

Synthesis and characterization of ferrocene-functionalized reduced graphene oxide nanocomposite as a supercapacitor electrode material

Reza Teimuri-Mofrad*, Raha Hadi, Hassan Abbasi

Department of Organic and Biochemistry, Faculty of Chemistry, University of Tabriz, Tabriz, Iran

ARTICLE INFO

Article history:
Received 3 October 2018
Received in revised form
4 November 2018
Accepted 26 November 2018
Available online 28 November 2018

Keywords:
Supercapacitor
Ferrocene
Graphene
Nanocomposite
Cycloaddition

ABSTRACT

A novel ferrocene-functionalized rGO as a electrode material is developed. The rGO was successfully functionalized through [1,2] cycloaddition reaction with 1,1′-bis(4-azidobutyl)ferrocene (bA-Fc). The functionalized ferrocene rGO nanocomposite (bA-Fc/rGO) has been completely characterized using FT-IR, EDX, XRD and SEM. The elimination of the strong azide stretching bond at ~2100 cm^{-1} in the FT-IR spectrum of bA-Fc/rGO nanocomposite obviously proved the cycloaddition reaction between bA-Fc and rGO. Its XRD pattern compared to the rGO indicated that the ferrocene moiety successfully functionlized on rGO. The structure of this nanocomposite was balled and wrinkled compared to the starting graphene oxide according to SEM analysis and XRD experiment. The EDX spectrum shows the existence of carbon, nitrogen, iron and oxygen elements in bA-Fc/rGO. The electrochemical properties of bA-Fc/rGO nanocomposite were investigated with CV, GCD and EIS measurements. The bA-Fc/rGO revealed a higher surface, electrochemical performances and electrical conductivity than rGO and bA-Fc. The bA-Fc/rGO nanocomposite showed very good stability in more than 2000 cycles and high rate capability. The results show that bA-Fc/rGO nanocomposite can be considered as a candidate to be used in supercapacitor electrode materials.

1. Introduction

During the last decades supercapacitors have possessed consideration, due to their high power density and long cycle life. According to energy storage mechanisms, supercapacitors are mainly classified in two types: pseudocapacitors and electrochemical double layer capacitors (EDLC). The pseudocapacitors supply energy using redox reactions between the electrolytes and electrode plate of conductive metal oxides (V_2O_5, RuO_2, and Co_3O_4) or conductive polymers [1–3]. EDLC reserve electric energy *via* charge segregation impound with electrostatic power in the interfacial double layer of an electrode material.

EDLCs electrodes are usually being made of carbon-based materials such as graphite, graphene, graphene oxide and carbon nanotubes (CNT), because of their electrical conductivity and large surface area. The graphene-based electrochemical double layer capacitors electrode materials have been studied extensively due to their conductivity and large surface [4–11]. So far, the applications of rGO have been devised in physics, chemistry, biochemistry, and biosensors, which still need more development. Graphene has been discovered in 2004 and since then, it has attracted enormous attentions giving to its predominant chemical, optical and electronic performance and wide potential range applications in nanomaterials and nanotechnology. The structural characteristic of a single-layer scaffold bearing two dimensional structures that accompanied with its high surface area, make it suitable for the construction of nanostructured hybrid materials.

However, the modification of such area with rGO derivatives possesses complex methods and improves summative effects to the underlying electrodes [12–17]. Ferrocene and ferrocene-functionalized compounds have been used as families of fascinating organic and organometallics compounds due to their redox properties [18]. In general, become of their relatively generation of stable redox systems, regeneration at low potential, and good electrochemical reversibility, they are well-known electron mediators [19–23]. In addition, other electrode materials with redox couple can also be considered to improve the speed capability of the pseudocapacitors.

With the best of our knowledge, there are a few graphene oxide ferrocene composites that are being applied as supercapacitors

* Corresponding author.
E-mail address: teimuri@yahoo.com (R. Teimuri-Mofrad).

https://doi.org/10.1016/j.jorganchem.2018.11.033
0022-328X/

[24]. Herein, we report the design and synthesis of ferrocene functionalized rGO by Refs. [1,2] cycloaddition reaction with ferrocene azide derivative for electrode materials.

2. Experimental

2.1. Materials

Synthetic grade dimethylformamide (DMF), *N*-methyl-2-Pyrrolidone (NMP), ethyl acetate, acetone, deionized water (DI), H_2SO_4, HCl, sodium azide, Na_2SO_4, graphite, $NaNO_3$, $KMnO_4$, hydrogen peroxide (30%), hydrazine monohydrate and silica gel were purchased from Merck and Sigma Aldrich chemicals and used without more purification.

2.2. Material characterization

NMR spectra were recorded with a Bruker FT-400 spectrometer. FT-IR spectra were recorded on a Bruker Tensor 27 spectrometer in/on KBr disks.

Elemental analysis (C, H, N) was performed on a Vario EL III analyzer. The morphologies and microstructures of the sample were characterized by scanning electron microscopy (SEM), energy-dispersive X-ray spectroscopy (EDX) (TESCAN MIRA3) and X-ray diffraction patterns (XRD) [(PANalytica X pertPRO, Germany) with Cu-Kα radiation (0.15406 nm) at accelerating voltage and current of 45 kV].

2.3. Synthesis of 1,1′-bis(4-chlorobutyl)ferrocene ***(4)***

Compound **4** was synthesized according to reported method in our previous works (Scheme 1) [18d,j].

2.4. Synthesis of ferrocene azide derivatives

Compound **4** (3 g, 9.5 mmol) and sodium azide (2 g, 61.5 mmol) were stirred for 2 days in DMF (50 mL) at room temperature (Scheme 1). The completion of reaction was monitored by TLC. After the completion of reaction the reaction mixture was washed with water and extracted with ethyl acetate (3 × 50 mL). The organic phases were combined and dried over $MgSO_4$ and removed in reduced pressure. The obtained crude product was purified on silica gel column chromatography with hexane/ethyl acetate (9/1) as eluent to give the corresponding products.

2.4.1. 1,1′-Bis(4-azidobutyl)ferrocene (bA-Fc) ***(5)***

Light brown viscous oil, 75% Yield. IR (KBr, cm^{-1}): 3085, 2932, 2860, 2094, 1347, 1034, 815, 494.^{1}H NMR (400 MHz, $CDCl_3$, ppm): 1.54–1.64 (m, 4H, $C\underline{H}_2C\underline{H}_2CH_2$-N), 2.35 (t, 2H, $J = 7$, Fc-$C\underline{H}_2$), 3.27 (t, 2H, $J = 6.6$, $C\underline{H}_2$-N_3), 3.96–3.99 (m, 8H, Cp). ^{13}C NMR (100 MHz, $CDCl_3$, ppm): 27.3, 27.6, 27.9 (CH_2), 50.2 ($\underline{C}$-N_3), 66.8, 67.6 (Cp), 87 (C_{Ipso}). Anal. Calc (%) for $C_{18}H_{24}N_6Fe$: C, 56.84; H, 6.22; N, 22.10; Fe, 14.73. Found: C, 56.62; H, 6.18; N, 22.15; Fe, 14.61.

2.4.2. 1- (4-azidobutyl)-1′-(4-chlorobutyl)ferrocene ***(6)***

Light brown viscous oil, 18% Yield. IR (KBr, cm^{-1}): 3083, 2931, 2859, 2095, 1450, 1351, 1263, 918, 816, 493.^{1}H NMR (400 MHz, $CDCl_3$, ppm): 1.53–1.67 (m, 6H, $C\underline{H}_2C\underline{H}_2CH_2$-$N_3$, $C\underline{H}_2CH_2CH_2Cl$), 1.76–1.89 (m, 2H, $C\underline{H}_2CH_2Cl$), 2.32–2.36 (m, 4H, Fc-$C\underline{H}_2$), 3.27 (t, 2H, J = 13, $C\underline{H}_2N_3$), 3.56 (t, 2H, J = 13, $C\underline{H}_2Cl$). ^{13}C NMR (100 MHz, $CDCl_3$, ppm): 27.3, 27.4, 27.6, 27.9, 31.3 (CH_2), (43.97 ($\underline{C}H_2Cl$), 50.30 ($\underline{C}H_2$-N_3), 66.9, 67.7 (Cp), 87.5 (C_{Ipso}). Anal. Calc (%) for $C_{18}H_{24}N_3ClFe$: C, 57.83; H, 6.43; N, 11.24; Fe, 15.00. Found: C, 57.68; H, 6.45; N, 11.30, Fe 15.11.

2.5. Preparation of the GO and rGO

Graphene oxide (GO) was prepared and purified using the Hummers method [25]. In a typical procedure, GO (0.2 g) was dispersed in 80 mL deionized water (DI) by ultrasonication for 1 h. Then, Hydrazine monohydrate (2 mL) was added to the obtained crude. The solution was stirred and heated in oil bath at 90 °C for 1 day. The reaction mixture was filtered and precipitates were washed with deionized water and ethanol for several times. Finally, purified rGO was dried in vacuum oven (Scheme 2).

2.6. Synthesis of ferrocene functionalized rGO nanosheets (bA-Fc/rGO)

The rGO (10 mg) was firstly dispersed into NMP (10 mL) and placed in a 25 mL flask fitted with a condenser. To the mixture, N_2 was bubbled for 15 min and then 300 mg of bA-Fc was added to the flask. Then, the mixture was heated at 160 °C for 1 day under N_2 flow. The solution was cooled to room temperature and the product (bA-Fc/rGO) was centrifuged, washed with DI water and ethanol for several times (Scheme 3) and dried in vacuum oven.

2.7. Preparation of electrode

1 mg of GO, rGO, or bA-Fc/rGO was dispersed into 1 mL of NMP under ultrasonic treatment in water bath at room temperature for 15 min. 2 μL of dispersant was then immobilized on a GC electrode by drop-coating. The drop-coated electrode was eventually dried under vacuum for 24 h.

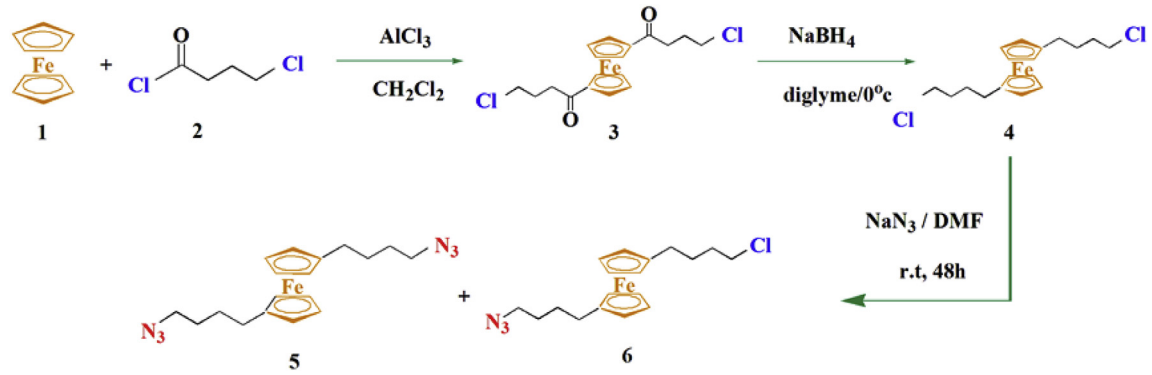

Scheme 1. Synthesis of 1,1′-bis(4-azidobutyl)ferrocene and 1-(4-azidobutyl)-1′-(4- chlorobutyl)ferrocene.

Scheme 2. Preparation of NPs–rGO.

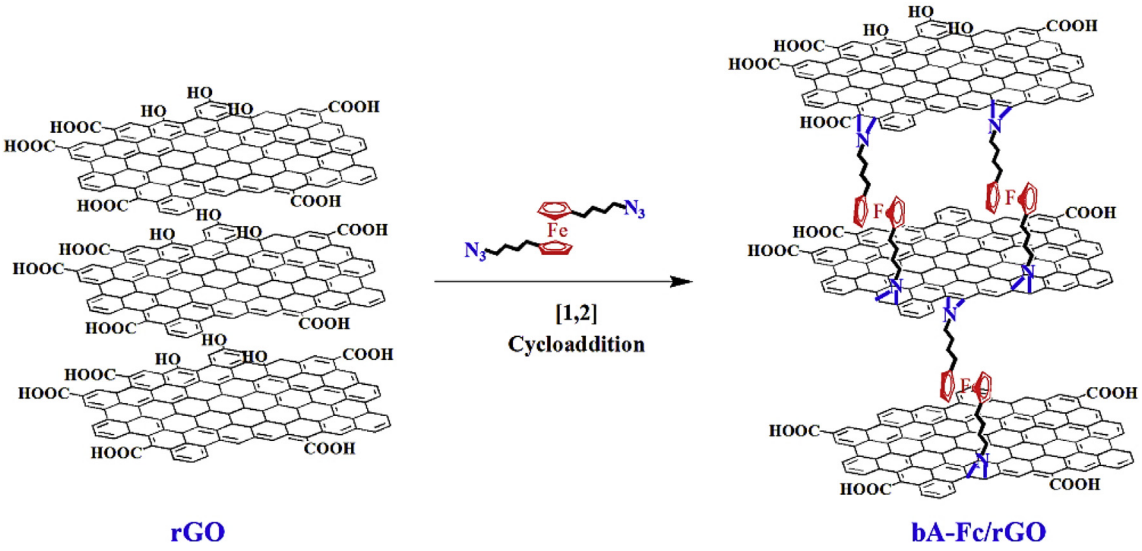

Scheme 3. Preparation of bA-Fc/rGO.

2.8. Electrochemical measurements

Electrochemical characterization of the prepared materials including cyclic voltammetry (CV) (AUTOLAB PGSTAT 30), galvanostatic charge-discharge measurements (GCD) and electrochemical impedance spectroscopy (EIS) (IVIUM S4A4 V99900) were performed in 1 M of H_2SO_4 electrolyte with the same equipment with a standard three electrode cell. A 2-mm-diameter GC was used as the working electrode. A platinum electrode and a silver/silver chloride (Ag/AgCl) electrode were used as the counter and the reference electrodes, respectively. The cyclic voltammetry curves were plotted with different scan rates from 10 to 200 mV s^{-1} between −0.8 and 0.9 V. Electrochemical impedance spectroscopy measurements were carried out in the frequency range from 100 kHz to 0.01 Hz in open circuit potential with an AC perturbation of 5 mV. The SC of the electrode material was calculated from the cyclic voltammetry curves and discharging curves according to equation (1). Fitting of the data were carried out with Zview software, where $\boldsymbol{q}^+$ and $\boldsymbol{q}^-$ are the voltammetric charges integrated from CV curves, $\boldsymbol{m}$ is the mass of the sponge electrode (bA-Fc/rGO nanocomposite) (g), $\boldsymbol{\Delta V}$ is the potential range in the CV (V).

$$C_{sp} = \frac{q^+ + |q^-|}{2\Delta V m} \quad (1)$$

3. Results and discussion

3.1. FT-IR analysis

FT-IR is one of the most well-known characterization procedures to elucidate the chemical structures. IR spectrum related to GO (Fig. 1a) displays the presence of different oxygen functional groups i.e. υ O-H at 3000-3500 cm^{-1}, υ C=O at 1750 cm^{-1} and υ C-O at 1000-1200 cm^{-1} and sp2-hybridized C=C vibrations. In the FT-IR spectrum of rGO (Fig. 1b), the intensity of the OH wide peak at ~3000-3500 cm^{-1} and the C-O peak at ~1080-1220 cm^{-1} is much less than GO.

Fig. 1c shows the FT-IR spectra of bA-Fc. As can be seen the appearance of new vibrational modes related to the C-N and C-O peaks at ~1271-1427 cm^{-1} in the bA-Fc, proved the cycloaddition reaction on rGO. The peak centered at 481 cm^{-1} is related to the ring-tilt of torsional vibration of ferrocene. In addition, elimination of the strong azide stretching bond at ~2100 cm^{-1} obviously proved the cycloaddition reaction between bA-Fc and rGO (Fig. 1d).

3.2. XRD analysis

The XRD patterns for GO, rGO and bA-Fc/rGO nanocomposite are illustrated in Fig. 2. The diffraction pattern of graphene oxide (Fig. 2a) exhibits a peak centered at $2\Theta = 14.3^\circ$ corresponding to a reflection (001) of graphite oxide. The disappearance of the (001)

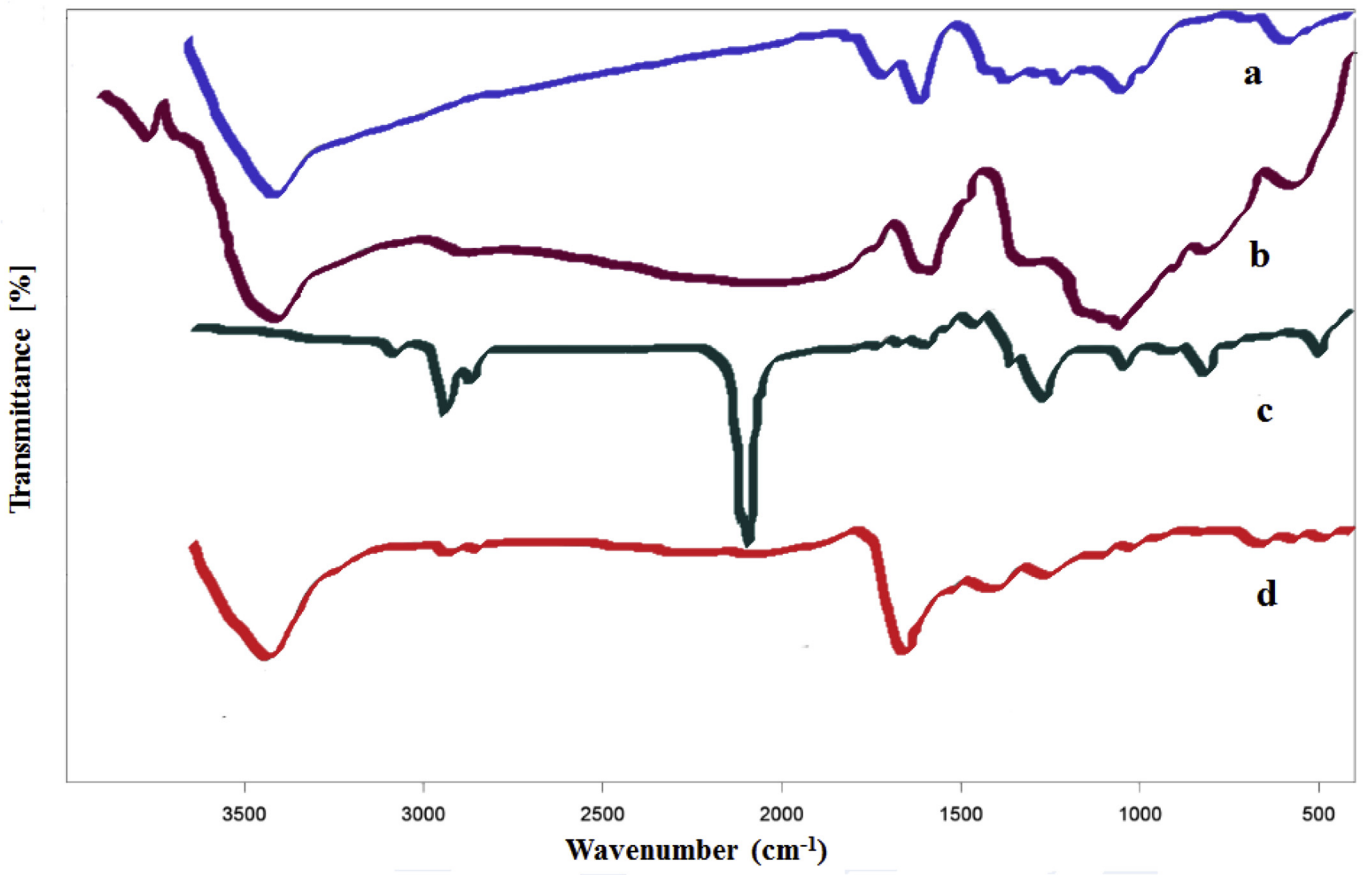

Fig. 1. FT-IR spectra of (a) GO, (b) rGO, (c) bA-Fc and (d) bA-Fc/rGO nanocomposite.

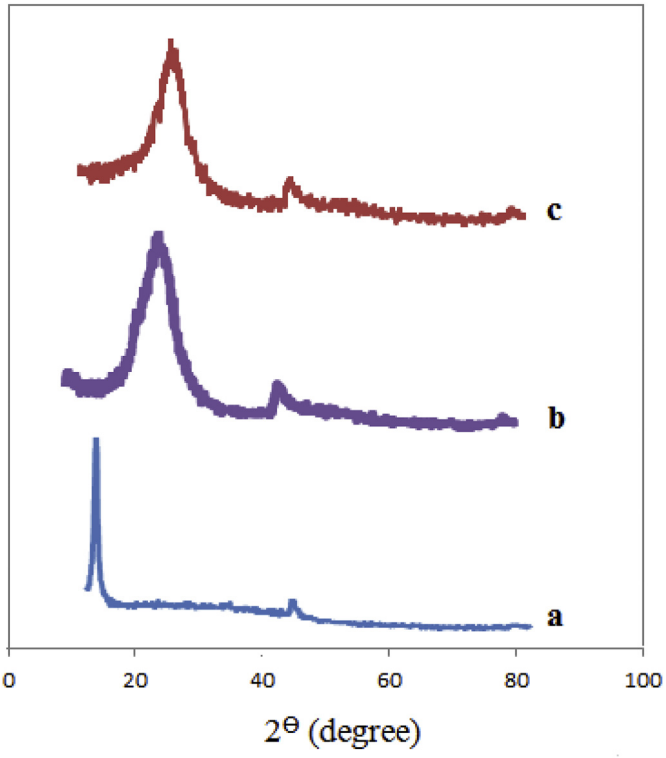

Fig. 2. XRD patterns of (a) GO, (b) rGO and (c) bA-Fc/rGO nanocomposites.

peak and the appearance of new diffraction peak at $2\Theta = 24^\circ$ in the XRD pattern of rGO (Fig. 2b) shows that graphene oxide was reduced well. The wide and faint peak at 2Θ of about 13° originated from the SiO_2 substrate used in XRD evaluation. XRD pattern of bA-Fc/rGO nanocomposite (Fig. 2c) exhibits five characteristic diffraction peaks at 2Θ values of 25°, 42°, 52°, 54° and 57°. It can be seen that the rGO and the ferrocene still have strong peaks indicating that they maintained their structures after rGO modification.

3.3. SEM and EDX analysis

The morphologies, shape and size of the GO, rGO and bA-Fc/rGO nanocomposite were studied by scanning electron microscopy (SEM) analysis (Fig. 3).

The structure of bA-Fc/rGO nanocomposite was observed to be balled and wrinkled compared to the starting graphene oxide (Fig. 3a–c). Modification of rGO with ferrocene seems that it has not changed the morphology of rGO and the unmodified morphology is still intact after functionalization. The bA-Fc/rGO nanocomposite could not be easily defined by SEM, which reveals the low conductivity of functionalized rGO. This can be explained by the [1,2] cycloaddition reaction leading to an opening rGO bandgap in a transition and a semi-metallic state to a semiconductor state that can be attributed to the modified π-conjugated network depends on the amount of aziridine groups.

The EDX spectrum of GO, rGO, bA-Fc and bA-Fc/rGO nanocomposite (Fig. 4) shows the existence of carbon (C), nitrogen (N), irons (Fe) and oxygen (O) elements.

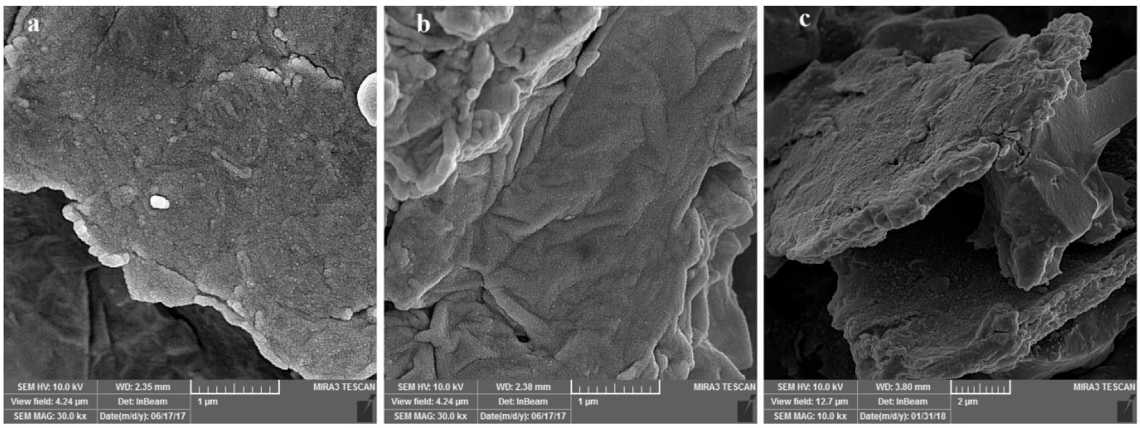

Fig. 3. SEM images of the (a) GO, (b) rGO and (c) bA-Fc/rGO.

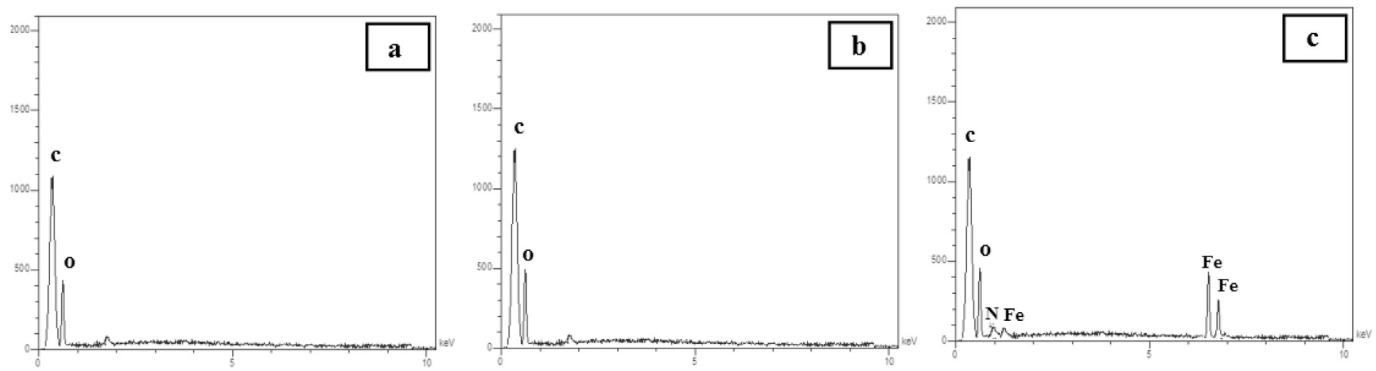

Fig. 4. EDX analysis of the (a) GO, (b) rGO and (c) bA-Fc/rGO.

3.4. Cyclic voltammetry studies

To evaluate the bA-Fc/rGO as a supercapacitor electrode material, the electrochemical properties tests were carried out using a three-electrode system with 1 M H_2SO_4 as the electrolyte. Fig. 5 shows CV curves of the GO, rGO, bA-Fc and bA-Fc/rGO nanocomposite electrode at different scan rates of 10–200 mV s^{-1}. Fig. 5 shows almost rectangular shapes with low redox protuberances at low scan rates, which are attributed to the redox reactions of the functional groups on the surface of GO and rGO (Fig. 5a–d). Fig. 5(c, d) shows the CV curves of bA-Fc and bA-Fc/rGO nanocomposite (scan rates 10 to 200 mVs^{-1}, voltage window of 1 V). The bA-Fc/rGO nanocomposite shows larger integrated areas in comparison to GO, rGO and bA-Fc. Besides, the redox peaks of Fc are seen at all scan rates. The CV curves of the bA-Fc/rGO nanocomposite show acceptable capacitive behavior than the GO, rGO and bA-Fc.

In addition to high rate capability, the cycle life test over 2000 cycles for bA-Fc/rGO nanocomposite was performed at a scan rate of 50 mV s^{-1} and the results are shown in Fig. 6. The bA-Fc/rGO nanocomposite electrode exhibits high cycling stability (89%).

3.5. EIS studies

The Nyquist plots of electrochemical impedance spectra (EIS) for rGO, bA-Fc and bA-Fc/rGO measured in the frequency range of 10^5–0.01 Hz are presented in Fig. 7. Two of Nyquist plots i.e. those of bA-Fc and bA-Fc/rGO exhibit a rather incomplete section of a semicircle. The equivalent electrical circuit (EEC) was depicted as the inset of Fig. 7 and the ZView® and fitted values of the circuit elements were gathered in Table 1. In this EEC, Rs (R_1) can be calculated as the intersection of semicircle on the high frequency end of real axis and the series resistance may be associated mainly to the intrinsic resistance of the active material. A constant phase element (CPE1) and a charge-transfer resistance (Rct) were included to describe the interfacial capacitance and charge transfer resistance associated with interfacial processes of counter ions through the electrode/electrolyte interface, respectively. Rct (R_2) can be calculated as the extrapolated diameter of the semicircle to low frequency region. As it can be seen from Table 1, the Rct value of bA-Fc/rGO was 14866 Ω, which was between those of bA-Fc (1.81E12 Ω) and rGO (5153 Ω). The straight line in the low frequency area was closer to being perpendicular to the real axis indicating an idealistic capacitor.

The deviation from electrochemical double layer is indicated by CPE, which is characterized by CPE-T (directly related to capacitance) and CPE-P (phase exponent which is 1 for an ideal capacitor). The CPE-T values, which are directly proportional to the interfacial specific capacitance of the electroactive material deposited on the electrode, were found in the order of bA-Fc/rGO > bA-Fc > rGO that suggest the higher capacitive behavior of bA-Fc/rGO.

3.6. Galvanostatic charge/discharge measurements studies

The best performance of bA-Fc/rGO nanocomposite supercapacitor was confirmed by GCD tests in a three-electrode system. It is illustrated the GCD for bA-Fc/rGO at several current densities varying from 1 to 20 Ag^{-1} in Fig. 8(b). The charge-discharge curves are almost symmetrical triangular with a slight curvature and a

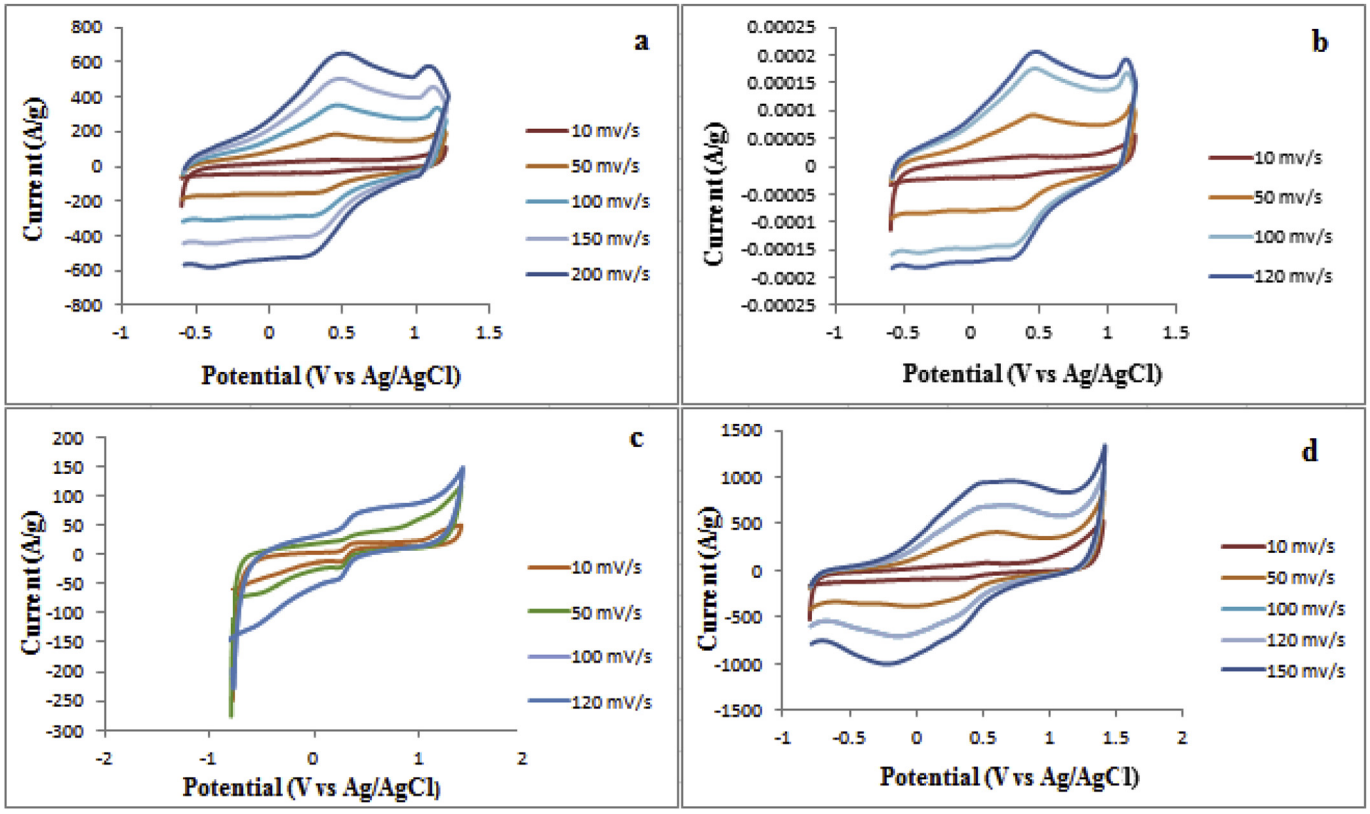

Fig. 5. CV curves of the (a) GO, (b) rGO, (c) bA-Fc and (d) bA-Fc/rGO nanocomposite at different scan rates from 10 to 100 mV s^{-1}.

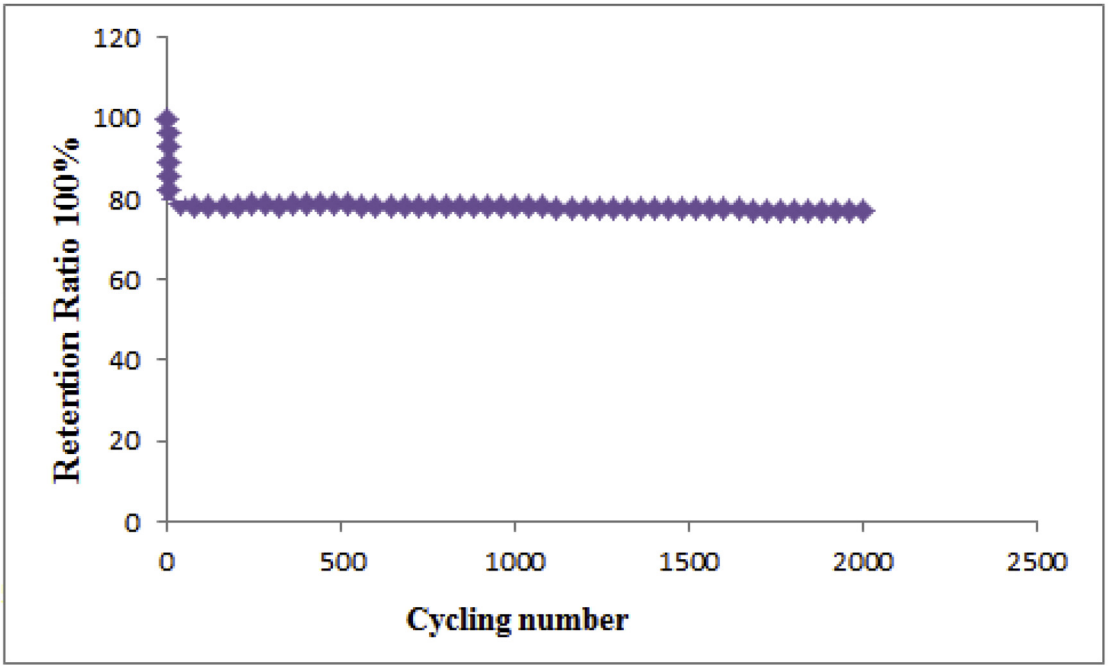

Fig. 6. Capacitance retention test over 2000 cycles at a scan rate of 50 mV s^{-1} for bA-Fc/rGO nanocomposite.

small iR drop is observed at a high current density of 20 Ag^{-1}. This behavior makes the bA-Fc/rGO nanocomposite a good candidate for using in supercapacitive device. However, once the current densities are less than 1 Ag^{-1}, an explicit platform can be obviously observed in the charge or discharge curve, which is due to the oxidation-reduction reversibility reaction for ferrocene in the bA-Fc/rGO nanocomposite. Charge–discharge curves of the rGO are shown in Fig. 8(a). In comparison with the rGO curves, the internal resistance (iR) of nanocomposite electrode bA-Fc/rGO was the smallest. The cycloaddition reaction between nitrene and double

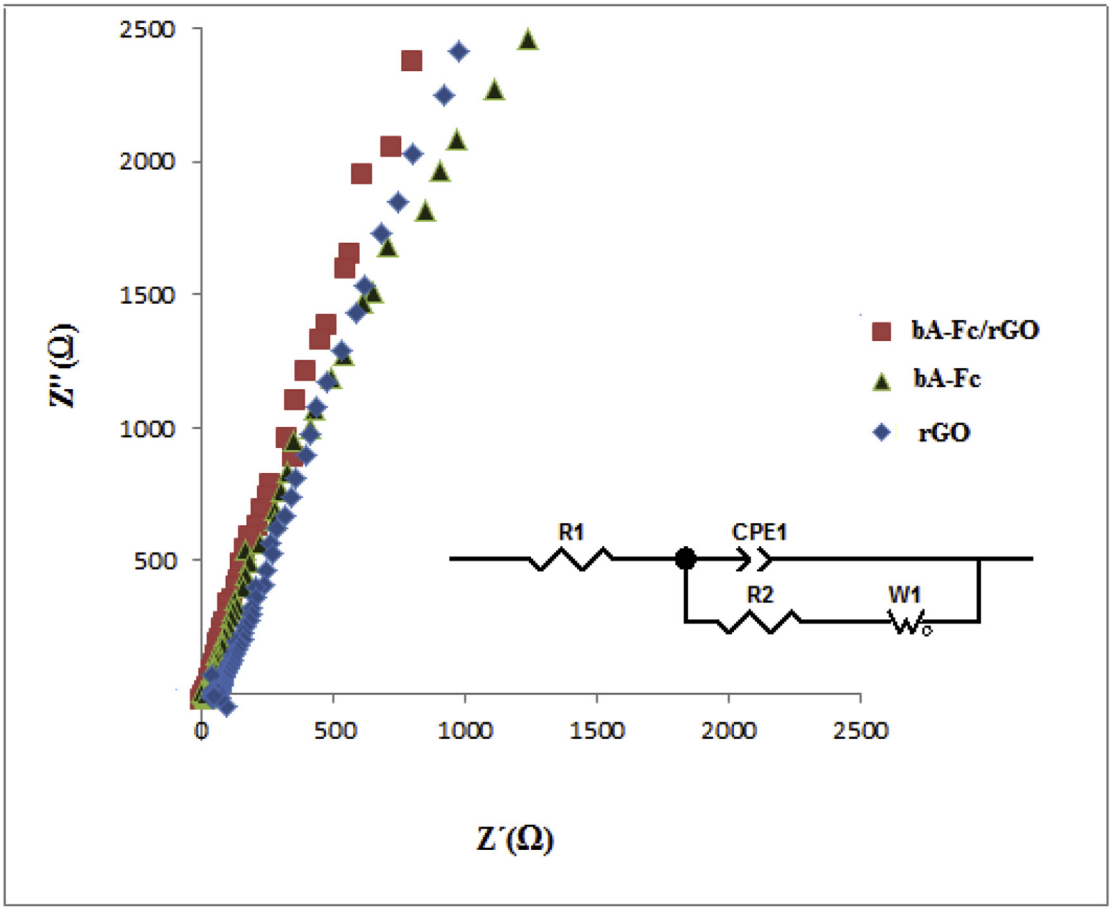

Fig. 7. Nyquist plots of electrochemical impedance spectra (EIS) of rGO, bA-Fc and bA-Fc/rGO nanocomposite.

Table 1
Values of the equivalent circuit elements based on the EIS analysis of rGO, bA-Fc and bA-Fc/rGO nanocomposite.

Sample	Rs	Rct	CPE	
			CPE-T	CPE-P
rGO	20.35	5153	0.000128	0.836
bA-Fc	62.11	1.81E12	0.00029	0.815
bA-Fc/rGO	16.81	14866	0.0004	0.767

bonds on rGO sheets significantly decreased the resistance of interface.

At higher current densities, the discharge time is down, which may be due to the limited availability of electrolyte ions [26]. The SC of the electrode bA-Fc/rGO nanocomposite is computed from the galvanostatic profiles of discharge using equation (2) [27], in which I is defined as the discharge current (A), Δt is the discharge time (s) and m is the mass of the active material (g).

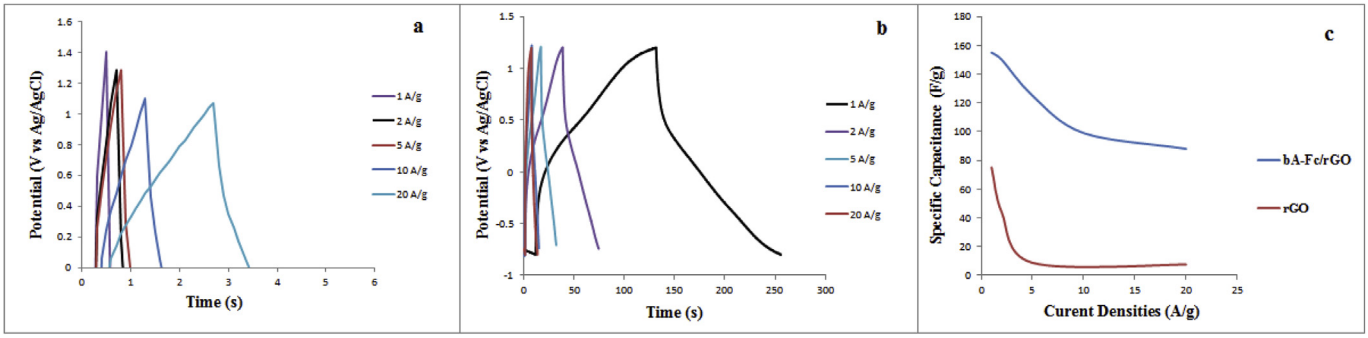

Fig. 8. (a) Charge-discharge curves at various current densities rGO, (b) Charge-discharge curves at various current densities for bA-Fc/rGO nanocomposite and (c) Average specific capacitance versus charge and discharge current density.

$$C_{sp} = \left[\frac{I\Delta t}{m\Delta V}\right] \quad \text{(Eq 2)}$$

The potential window shows with $\boldsymbol{\Delta V}$ (V). The SC of the bA-Fc/rGO electrode is lower at high current density and higher at low current density (Fig. 8c), and this is due to the following reason: at higher current density, electrolytes do not accessibility to the internal surface of the electrode material due to time constraints, while at low current density, the electrolyte ions have appropriate time to adsorb/desorb on the internal and external surface of the active material [26].

It is clear that all the curves have a small ohmic drop at the beginning of the discharge state, and this clarifies that the nanocomposites have an equivalent series resistance (ESR). However, the potential drop became smaller with the functionalization the reduced graphene oxide by 1,1′-bis(4-azidobutyl)ferrocene, benefiting from the good electrical conductivity of them. The charge–discharge curves in Fig. 8 are linear, triangular shaped, very sharp and symmetric. These indicate the reversible behavior.

4. Conclusions

In summary, we have functionalized the reduced graphene oxide by 1,1′-bis(4-azidobutyl)ferrocene, using nitrene chemistry for applying in electrode materials. Systematic electrochemical experiments show that the bA-Fc/rGO nanocomposite significantly improves the cycling resistance, with much better capacitance retention than the GO, rGO and bA-Fc. The electrochemical behaviors of bA-Fc/rGO nanocomposite were characterized by CV, GCD and EIS measurements. The high capacitance and rate capability of the synthesized bA-Fc/rGO supercapacitor is due to the low resistance response and very reversible faradaic redox of the bA-Fc/rGO nanocomposite.

Acknowledgements

This research was financial supported by the Research Council of University of Tabriz, Iran.

Appendix A. Supplementary data

Supplementary data to this article can be found online at https://doi.org/10.1016/j.jorganchem.2018.11.033.

References

[1] R. Kötz, M. Carlen, Principles and applications of electrochemical capacitors, Electrochim. Acta 45 (2000) 2483–2498.
[2] M. Winter, R.J. Brodd, What are batteries, fuel cells, and supercapacitors? Chem. Rev. 104 (2004) 4245–4269.
[3] H. Jeon, B. Jeong, J.K. Lee, H.S. Kim, S.H. Lee, J. Lee, Improved specific capacitance of amorphous vanadium pentoxide in a nanoporous alumina template, Electrochem. Solid State Lett. 13 (2010) 25–28.
[4] L. Dai, Functionalization of graphene for efficient energy conversion and storage, Acc. Chem. Res. 46 (2013) 31–42.
[5] X. Sun, P. Cheng, H. Wang, H. Xu, L. Dang, Z. Liu, Z. Lei, Activation of graphene aerogel with phosphoric acid for enhanced electrocapacitive performance, Carbon 92 (2015) 1–10.
[6] R.R. Salunkhe, Y. Kamachi, N.L. Torad, S.M. Hwang, Z. Sun, S.X. Dou, J.H. Kim, Y. Yamauchi, Fabrication of symmetric supercapacitors based on MOF-derived nanoporous carbons, J. Mater. Chem. 2 (2014) 19848–19854.
[7] G. Xiong, C. Meng, R.G. Reifenberger, P.P. Irazoqui, T.S. Fisher, A review of graphene-based electrochemical microsupercapacitors, Electroanalysis 26 (2014) 30–51.
[8] R.R. Salunkhe, J. Lin, V. Malgras, S.X. Dou, J.H. Kim, Y. Yamauchi, Large-scale synthesis of coaxial carbon nanotube/Ni(OH)$_2$ composites for asymmetric supercapacitor application, Nanomater. Energy 11 (2015) 211–218.
[9] Z. Chen, V. Augustyn, J. Wen, Y. Zhang, M. Shen, B. Dunn, Y. Lu, High-performance supercapacitors based on intertwined CNT/V_2O_5 nanowire nanocomposites, Adv. Mater. 23 (2011) 791–795.
[10] Y. Lv, H. Wang, X. Xu, J. Shi, W. Liu, X. Wang, Balanced mesoporous nickle cobaltite-graphene and doped carbon electrodes for high-performance asymmetric supercapacitor, Chem. Eng. J. 326 (2017) 401–410.
[11] R.R. Salunkhe, Y.V. Kaneti, J. Kim, J.H. Kim, Y. Yamauchi, Nanoarchitectures for metal–organic framework-derived nanoporous carbons toward supercapacitor applications, Acc. Chem. Res. 49 (2016) 2796–2806.
[12] T. Gan, S. Hu, Electrochemical sensors based on graphene materials, Microchim. Acta 175 (2011) 1.
[13] A. Rochefort, J.D. Wuest, Interaction of substituted aromatic compounds with graphene, Langmuir 25 (2009) 210–215.
[14] C.S. Shan, H.F. Yang, J.F. Song, D.X. Han, A. Ivaska, L. Niu, Direct electrochemistry of glucose oxidase and biosensing for glucose based on graphene, Anal. Chem. 81 (2009) 2378–2382.
[15] H.J. Choi, S.M. Jung, J.M. Seo, D.W. Chang, L. Daic, J.B. Baek, Graphene for energy conversion and storage in fuel cells and supercapacitors, Nanomater. Energy 1 (2012) 534–551.
[16] M. Pumera, A. Ambrosi, A. Bonanni, E.L.K. Chng, H.L. Poh, Graphene for electrochemical sensing and biosensing, Trends Anal. Chem. 29 (2010) 954–965.
[17] K.S. Novoselov, A.K. Geim, S.V. Morozov, D. Jiang, Y. Zhang, S.V. Dubonos, L.V. Grigorieva, A.A. Firsov, Electric field effect in atomically thin carbon films, Science 306 (2004) 666–669.
[18] a) K.D. Safa, H. Abbasi, R. Teimuri-Mofrad, Synthesis of novel ferrocenyl silyl ethers via dehydrocoupling reactions under Karstedt catalyst, J. Organomet. Chem. 740 (2013) 56–60;
b) R.F. Teimuri-Mofrad, Mirzaei, H. Abbasi, K.D. Safa, Synthesis of new binuclear ferrocenyl compounds by hydrosilylation reactions, C. R. Chimie. 20 (2017) 197–205;
c) K.D. Safa, H. Abbasi, R. Teimuri-Mofrad, F.A. Charandabi, Aust. J. Chem. 67 (2014) 784–789;
d) R. Teimuri-Mofrad, H. Abbasi, K.D. Safa, B. Tahmasebi, Synthesis of novel bis [(tris(dimethylsilyl)methyl) alkyl]ferrocene derivatives as new ferrocenyl multi-functional silyl ether compounds, ARKIVOC 4 (2016) 371–384;
e) R. Teimuri-Mofrad, K. Rahimpour, R. Ghadari, Synthesis, characterization, and electronic properties of novel Fc-DCM conjugated system; experimental and computational studies, J. Organomet. Chem. 811 (2016) 14–19;
f) R. Teimuri-Mofrad, K. Rahimpour, R. Ghadari, Design, synthesis and characterization of ferrocene based V-shaped chromophores with modified nonlinear effect, J. Organomet. Chem. 846 (2017) 397–406;
g) R. Teimuri-Mofrad, K. Rahimpour, R. Ghadari, S. Ahmadi-Kandjani, Ferrocene based nonlinear optical chromophores: synthesis, characterization and study of optical properties, J. Molecular liquid 244 (2017) 322–329;
h) R. Teimuri-Mofrad, K. Rahimpour, A.R. Vaez, Isophorone-based organometallic chromophores: synthesis, characterization and investigation of electro-optical properties, Appl. Organomet. Chem. 32 (2017) e4031;
i) R. Teimuri-Mofrad, K. Rahimpour, A. Poursadegh, Nvestigation of 5,6-dimethoxy-1-indanone derivatives in optical applications: synthesis, characterization and study of linear and nonlinear optical properties, Mater. Chem. Phys. 200 (2017) 384–394;
j) R. Teimuri-Mofrad, K.D. Safa, K. Rahimpour, Synthesis, characterization and electrochemical properties of novel trinuclear ferrocenyl based organosilane compounds, J. Organomet. Chem. 758 (2014) 36–44.
[19] G. Tan, Z. Cheng, Y. Qiu, W. Huang, H. Fan, B. Ren, Supercapacitors based on polyelectrolyte/ferrocenyl-surfactant complexes with high rate capability, RSC Adv. 6 (2016) 31632–31638.
[20] G. Kalita, S. Sharma, K. Wakita, M. Umeno, Y. Hayashi, M. Tanemura, A photoinduced charge transfer composite of graphene oxide and ferrocene, Phys. Chem. Chem. Phys. 15 (2013) 1271–1274.
[21] R.S. Dey, R. Raj, Redox-functionalized graphene oxide architecture for the development of amperometric biosensing platform, ACS Appl. Mater. Interfaces 5 (2013) 4791–4798.
[22] K. Deng, J. Zhou, X. Li, Noncovalent nanohybrid of ferrocene with chemically reduced graphene oxide and its application to dual biosensor for hydrogen peroxide and choline, Electrochim. Acta 95 (2013) 18–23.
[23] L. Fan, Q. Zhang, K. Wang, F. Li, L. Niu, Ferrocene functionalized graphene: preparation, characterization and efficient electron transfer toward sensors of H_2O_2, J. Mater. Chem. 22 (2012) 6165–6170.
[24] a) A. Rabti, C.C. Mayorga-Martinez, L. Baptista-Pires, N. Raouafi, A. Merkoçi, Ferrocene-functionalized graphene electrode for biosensing applications, Anal. Chim. Acta 926 (2016) 28–35;
b) G. Tan, Z. Cheng, Y. Qiu, W. Huang, H. Fan, B. Ren, Supercapacitors based on polyelectrolyte/ferrocenylsurfactant complexes with high rate capability, RSC Adv. (2016) 1–10;
c) M. Liu, L. Wang, J. Deng, Q. Chen, Y. Li, Y. Zhang, H. Li, S. Yao, Highly sensitive and selective dopamine biosensor based on a phenylethynyl ferrocene/graphene nanocomposite modified electrode, Analyst 137 (2012) 4577–4583.
[25] W.S. Hummers, R.E. Offeman, Preparation of graphitic oxide, J. Am. Chem. Soc. 80 (1958), 1339-1339.
[26] R. Madhu, K. Vijaya Sankar, S.M. Chen, R. Kalaiselvan, Eco-friendly synthesis of activated carbon from dead mango leaves for the ultrahigh sensitive detection of toxic heavy metal ions and energy storage applications, RSC Adv. 4 (2014) 1225–1233.
[27] K. Krishnamoorthy, G.K. Veerasubramani, S. Radhakrishnan, S.J. Kim, One pot hydrothermal growth of hierarchical nanostructured Ni_3S_2 on Ni foam for supercapacitor application, Chem. Eng. J. 251 (2014) 116–122.